J Mater Sci (2009) 44:1622–1632
DOI 10.1007/s10853-008-3228-3

Effect of microstructure on the fatigue behavior of aluminum titanate ceramics

Tsuneaki Matsudaira · Yoshihisa Matsumura · Satoshi Kitaoka · Hideo Awaji

Received: 2 April 2008 / Accepted: 23 December 2008 / Published online: 27 January 2009

Abstract The effect of microstructures, such as grain size and internal pores, on the fatigue behavior of aluminum titanate (AT, Al_2TiO_5) ceramics was investigated at room temperature and 973 K. When the average grain size of the AT ceramics was decreased from 22 to 13 μm, the flexural strength was approximately doubled at both temperatures. The decrease in the grain size is considered to reduce the size and amount of microcracks present at the grain boundaries. Fatigue deterioration of the ceramics was accelerated by applying cyclic stress. The cyclic fatigue behavior of the ceramics with smaller grains suggested control by a "grain bridging degradation mechanism" at both temperatures. However, that of the ceramics with larger grains was governed by the fatigue mechanism, depending on the testing temperatures. There was little effect from internal pores on the cyclic fatigue behavior of the AT ceramics at room temperature. On the other hand, at 973 K, the lifetime of the cyclic fatigue was decreased due to the presence of pores.

Introduction

Aluminum titanate (AT, Al_2TiO_5) ceramics are promising candidates for use as casting tools in contact with molten aluminum alloys, because they have excellent thermal shock resistance and adequate non-wettability to molten aluminum [1]. The guarantee of reliability has become a requirement for AT ceramics, because of their significantly low mechanical strength compared with general structural ceramics, and because productivity requirements for larger casting parts with few defects have become greater.

The excellent thermal shock resistance of AT ceramics is a result of the presence of many microcracks along the grain boundaries due to the large anisotropic thermal expansion [2] of AT crystal during cooling after sintering, but which leads to the degradation of flexural strength. The morphology of microcracks in AT ceramics show remarkable temperature dependence; the microcracks are open at room temperature, but those at grain boundaries close up with increasing temperatures. At still higher temperatures, the grains of AT ceramics are bonded together through a glassy layer existing at the grain boundaries [2–5].

Because such microcracks generally shorten the fatigue lifetime of ceramics, [6] and the grain size of the AT ceramics directly influences the amount of microcracks and the microcrack opening width [4, 5], it is predicted that the fatigue behavior of AT ceramics is strongly affected by the grain size, and the temperature of application. Therefore, AT ceramics have not been utilized as engineering parts, because of their very low flexural strength. There are a few studies that have quantitatively analyzed the fatigue properties of AT ceramics. We have investigated the fatigue degradation mechanism of AT ceramics, and determined its relation with the morphological changes of the microcracks, which are dependent on the temperature [7, 8]. However, there have been no reports regarding the dependence of fatigue behavior on the grain size of AT ceramics.

Ceramic parts with complex shapes, such as ladles and stokes for the aluminum casting tools, are often manufactured by slip-casting, and many pores are frequently

T. Matsudaira (✉) · S. Kitaoka
Japan Fine Ceramics Center, 2-4-1 Mutsuno, Atsuta-ku, Nagoya 456-8587, Japan
e-mail: matsudaira@jfcc.or.jp

Y. Matsumura · H. Awaji
Nagoya Institute of Technology, Gokiso-cho, Showa-ku, Nagoya 466-8555, Japan

introduced into the molded parts during casting. However, the effect of pores on the fatigue properties of AT ceramics containing microcracks is completely unknown. If this effect is clarified, it will be possible to propose an appropriate direction for improvement of the manufacturing method and use of AT ceramic parts.

In this study, the effect of microstructures, such as grain size and internal pores, on the fatigue behavior of AT ceramics was investigated, and the fatigue mechanism was considered from the viewpoint of the morphological change in microcracks, which exhibits remarkable dependence on the exposure temperatures.

Experimental procedures

Three kinds of straight slip-cast AT ceramic pipes (length: 930 mm, thickness: 10 mm, Marusu Glaze Co., Japan) were used. These pipes (samples I–III) contain an aluminum silicate glassy phase (added as a sintering aid) segregated at the grain boundaries. The grain size of the AT ceramics can be sensitively controlled by the insubstantial amount of SiO_2, which is the main component of the glassy phase. Sample II was prepared by increasing the SiO_2 content by a few percent compared to that of sample I. The major axis length and area of each Al_2TiO_5 grain (total number of grains = 1,200) were measured for the mirror-like surfaces of the samples. The average grain size of the samples was determined from the major axis length that corresponds to a cumulative area ratio of 50%.

Figure 1 shows scanning electron microscopy (SEM) images of the microstructures and the corresponding grain size distribution of samples I and II. The average grain sizes of sample I, described in previous articles, [7, 8] and sample II are 22 and 13 μm, respectively.

The raw powders used for the preparation of sample III were the same as those for sample II. Although the average grain size of sample III is almost the same as that of sample II, many internal pores were introduced by the addition of a bubbling agent. Figure 2 shows SEM images of typical fracture surfaces for samples II and III. The arrow in Fig. 2b indicates one of a large number of the internal spherical pores introduced during the slip-casting of sample III. Few pores are observed on the fracture surface of sample II; however, for sample III, there are many spherical pores of approximately 50 μm in diameter with submillimeter intervals.

The flexural strength and fatigue behavior of AT ceramics are significantly affected by morphological changes in the microcracks at the grain boundaries. The amount of microcracks and their opening widths depend strongly on the temperature to which the ceramics were exposed. Thus, the temperature dependences of the thermal conductivity and the elastic modulus of the samples were investigated to evaluate the effect of the testing temperature.

Figure 3 shows the temperature dependence of thermal conductivity and the elastic modulus of the AT ceramic samples. The thermal conductivities of the samples (ϕ 10 mm × 1 mm) were measured in a temperature range

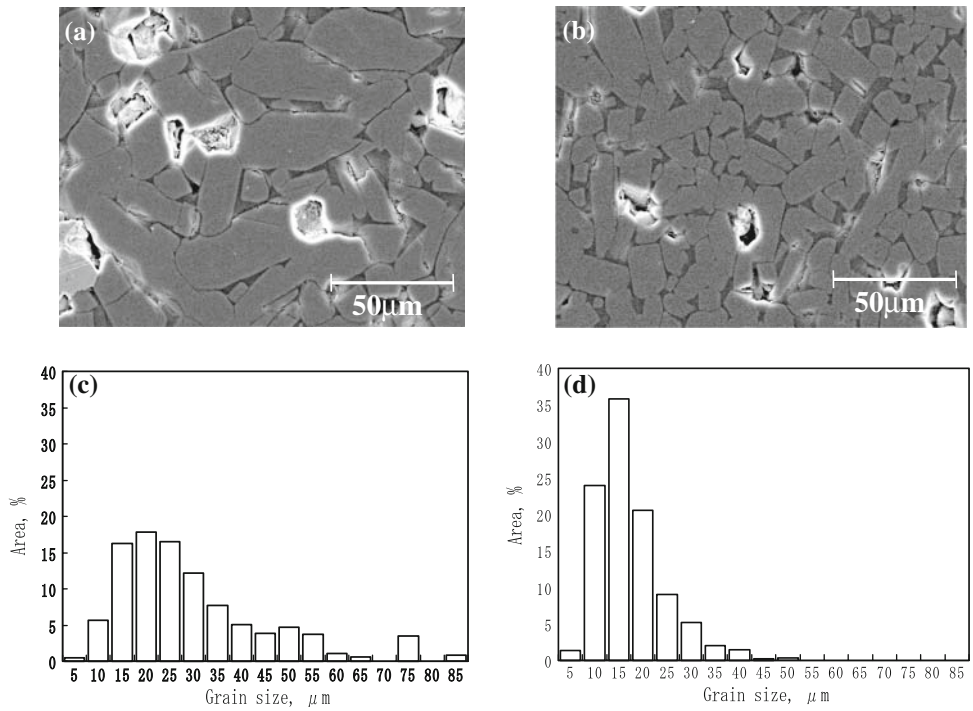

Fig. 1 SEM images of the microstructures and grain size distributions of samples I (**a**, **c**) and II (**b**, **d**)

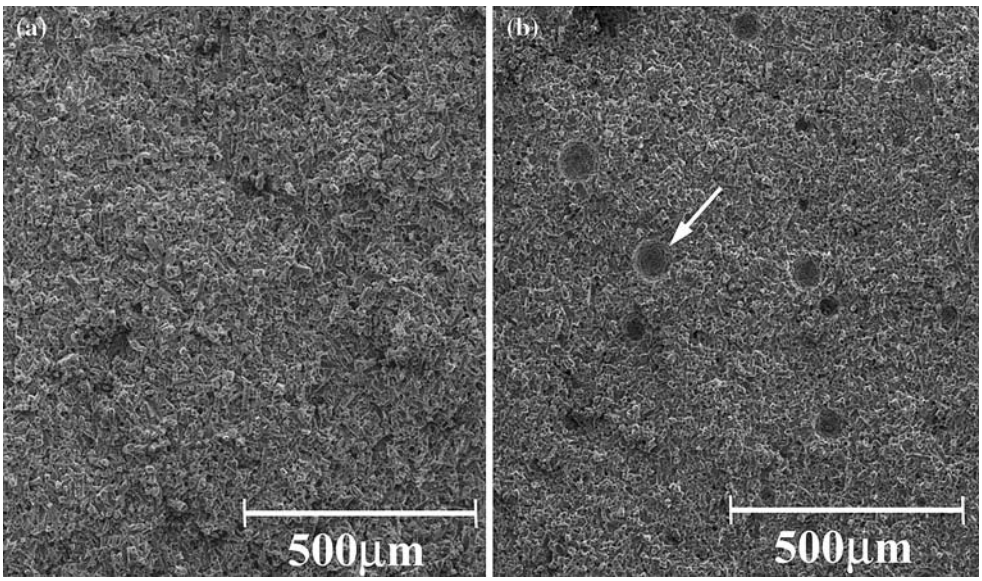

Fig. 2 SEM images of typical fracture surfaces of specimens tested at room temperature for (**a**) samples II and (**b**) III. Arrow indicates one of a large number of the internal spherical pores introduced during the slip-casting of sample III

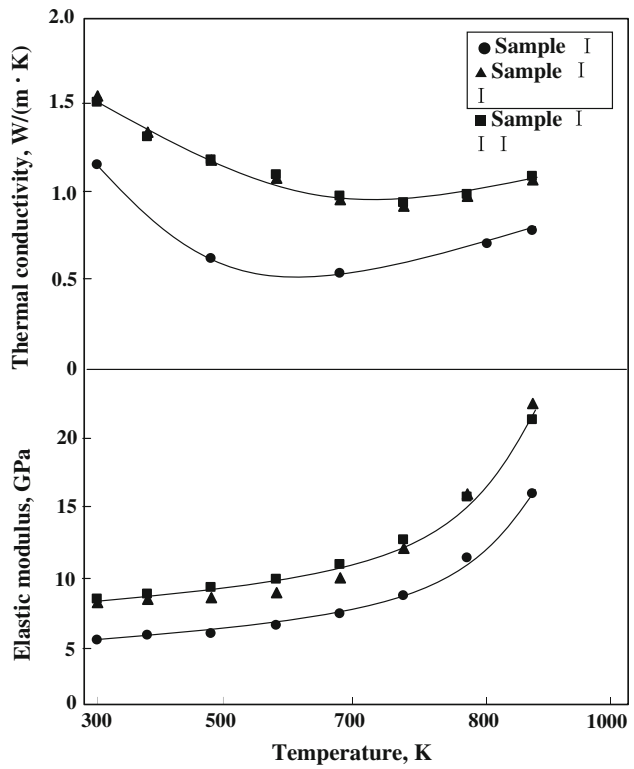

Fig. 3 Temperature dependence of thermal conductivity and elastic modulus for the AT ceramics

from RT to 1,073 K by the laser-flash method specified by JIS R 1611 [9]. The elastic moduli of the samples (100 × 20 × 1 mm) were measured at temperatures from RT to 973 K by the flexural resonance method specified by JIS R 1605 [10].

All of the samples show a decrease in thermal conductivity with increasing temperature to a minimum in the range of 600–700 K, followed by an increase with increasing temperature. The decrease in thermal conductivity is caused by the increase of phonon scattering. Increasing thermal conductivity beyond the range of 600–700 K is related to the increment of the heat transfer paths due to shielding of the intergranular microcracks, which is caused by the anisotropic expansion of AT grains along the direction of the a and b axes, the thermal expansion coefficients of which show positive values. On the other hand, the elastic moduli increase gradually with increasing temperature, and increase rapidly above 700 K, which is thought to contribute to microcrack shielding. Both the thermal conductivity and elastic modulus of sample II are higher than those of sample I. Because the grain size of sample II is smaller than that of sample I, the amount of cracks and the crack opening width in sample II are probably less than those of sample I, which may result in the ease of the microcrack closing of sample II with the increase in temperature. The microcracks of all the samples are, in any event, considered to be opening at room temperature and shielded at 973 K, at which temperature the AT ceramics are used as parts in contact with molten aluminum alloys. In addition, the thermal conductivity and elastic modulus of samples II and III are almost the same. Therefore, the thermal conductivity and elastic modulus for the temperatures between room temperature and 973 K are not affected by the pores introduced during the casting.

The AT ceramics that contain a large amount of microcracks have very low flexural strengths. For this reason, bar-shaped specimens with dimensions of 7.5 × 5 × 40 mm

were cut from the samples for the fatigue tests to ensure that the minimum applied load could be controlled during the cyclic fatigue tests using a load cell with a lower detection limit of 0.025 N. Each specimen was set in a three-point bending jig, where the tensile surface was 5 × 40 mm and the lower span was 30 mm. The flexural strength was measured at room temperature and 973 K under a cross-head speed of 0.5 mm/min. Cyclic fatigue tests were carried out at room temperature and 973 K in air at a frequency of 20 Hz with sinusoidal loading cycles of constant amplitude until the number of cycles, N, reached 2×10^6. The load ratio, R ($=R_{min}/R_{max}$), was 0.1. Static fatigue tests were also performed under constant loads at the same temperatures. The upper limit of the testing duration was 100.000 s. Ten specimens were used at each stress level for the cyclic and static fatigue tests, except those at 973 K where only five specimens were used.

The fatigue data obtained under each testing condition were statistically analyzed by the same method as previously described [7, 8, 11, 12]. The Weibull distribution was plotted using all of the fatigue data which consist of perfect and imperfect data. Perfect data refer to those specimens that fractured during the fatigue tests, and the imperfect data refer to those specimens that failed before the maximum stress was reached, or survived to the end of the test. The median values of the apparent lifetime were determined by a least square approximation using only the perfect data. The imperfect data were used only for counting the order in the Weibull distribution.

A fatigue limit at room temperature, where the maximum applied stress corresponds to no strength degradation during the fatigue tests, was also statistically estimated [7, 8, 11, 12]. The flexural strength and residual strength of the specimens surviving the cyclic fatigue tests at room temperature were measured in Ar at the same temperature, in order to prevent subcritical crack growth due to stress corrosion cracking. The Weibull distribution was plotted using all of the residual strength data, which consist of perfect and imperfect data. Perfect data refers to the residual strength obtained by survived specimen to the end of the fatigue test, and the imperfect data refers to those specimens that fractured during the fatigue tests. The median values of the apparent residual strength were determined by a least square approximation using only the perfect data. The imperfect data were used only for counting the order in the Weibull distribution. Next, the relationship between the residual strength and the maximum applied stress was plotted. The fatigue limit of the AT ceramics under the cyclic stresses was statistically estimated from the intersection of the average inert strength and the extrapolation of the line obtained by plotting residual strength as a function of the maximum applied stress. The fracture surfaces of those specimens that failed during the fatigue tests were examined using SEM.

Results and discussion

Flexural strength

Figure 4 shows typical load–displacement curves during the three-point bending tests. For the specimens tested at room temperature, the curves do not show an obvious initial linear elastic region before attainment of the maximum load which is then followed by a continuous load decrease. The specimens were not separately broken even after the bending tests. Although the maximum loads for samples II and III are approximately twice that of sample I, the corresponding displacements slightly decreased. For the specimens tested at 973 K, the maximum loads are twice or more as those that are obtained at room temperature. The displacements up to maximum load for samples II and III are smaller than that for sample I, which is similar to those tested at room temperature. As Fig. 4 shows, the load–displacement curves at 973 K of all the samples have an initial linear elastic region, followed by an increasingly nonlinear region up to a maximum load, and then followed by a sudden reduction due to the rapid propagation of the main crack. For samples I and II, however, the crack was arrested near the compression side of the specimens, followed by a continuous load decrease. Such crack arrest did not occur for sample III, which broke completely.

The decrease in the grain size results in the increase of the flexural strength at both temperatures; however, it does not lead to a significant increase in the fracture energy. The increment of the flexural strength due to the decrease in grain size is probably related to the decrease in the amount of microcracks and the microcrack opening width. This was suggested as due to both the thermal conductivity and elastic modulus of samples II and III being larger than those of sample I, as shown in Fig. 3. The increase in flexural strength due to the increase of temperature is

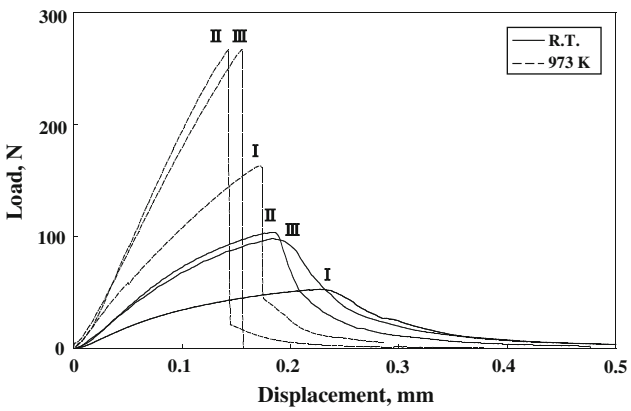

Fig. 4 Typical load–displacement curves during three-point bending tests of sample I, II, and III specimens at room temperature and 973 K

considered to be caused by microcrack closure, as predicted by Fig. 3.

The thermomechanical properties and the load–displacement curves of the sample III shown in Figs. 3, 4 are almost the same as those of sample II. These properties of AT ceramics are not affected by the internal large pores introduced during slip-casting. At room temperature, the microcracks at grain boundaries are fully open; therefore, macroscopic cracks are probably formed by the connection of microcracks with each other, and the introduced pores cannot act as an origin of fracture. On the other hand, at 973 K, the microcracks are shielded, as observed from Fig. 3; however, the surfaces of the microcracks may not attain a state where they adhere to each other through the soften glassy layer. Therefore, when external stress is applied to the specimens, they may be easily deformed by a slight slip in the AT grains, followed by the formation of large cracks without stress concentration at the pores.

Effect of grain size

Figure 5 shows the maximum stresses as a function of the apparent lifetime to fracture during cyclic fatigue tests of the sample II at room temperature and 973 K. Open rhombic symbols indicate the median values of the apparent lifetime distributions. Filled circles indicate the fatigue data for the specimens that fractured during the tests, and the number of specimens that survived to the end of the tests are indicated by arrows with the corresponding number of specimens. The dotted lines indicate the median values of the flexural strength distributions tested at each temperature. The apparent lifetimes at both temperatures, when the specimens failed during the tests, increase as the maximum stress decreases. The maximum stresses-to-fatigue fracture for sample II were approximately twice as large as sample I at both temperatures [7, 8], similar to the flexural strength shown in Fig. 4.

Figure 6 shows applied stresses as a function of the lifetime to fracture during static fatigue tests of sample II at room temperature and 973 K. Open rhombic symbols indicate the median values of the apparent lifetime distributions. Filled circles indicate the fatigue data for the specimens. Those samples with arrows pointing to the left indicate specimens that failed before their maximum stress was reached. The dotted lines, filled circles, and arrows pointing to the right with numbers have the same denotations as those in Fig. 5. Although the lifetimes at room temperature obviously increase with decreasing applied stress, those at 973 K are not dependent on the stress, and the specimens either failed up to the maximum load of the fatigue tests, or did not fail after arrival at the upper limit of testing time. This fracture behavior was similar to that for sample I previously described [7, 8].

Figure 7 compares a summary of the stress–lifetime curves of sample II and I obtained from the median values of the cyclic and static fatigue distributions obtained in air at room temperature and 973 K. In the case of the cyclic fatigue data, the apparent fatigue lifetime was calculated from the multiplication of the number of cycles, N, and the period. Because the median values for the static fatigue lifetimes at 973 K could not obtained as shown in Fig. 6, no data are shown for this temperature in Fig. 7. The cyclic fatigue lifetimes can be directly compared with the static fatigue lifetimes applying the following correction, g_m:

$$g_m = \frac{1}{\lambda}\int_0^{\lambda}\left(\frac{\sigma(t)}{\sigma_{max}}\right)^{n_C} dt \qquad (1)$$

where σ_{max} is the maximum value of the applied cyclic stress, $\sigma(t)$, λ is the cyclic period, and n_c is the cyclic

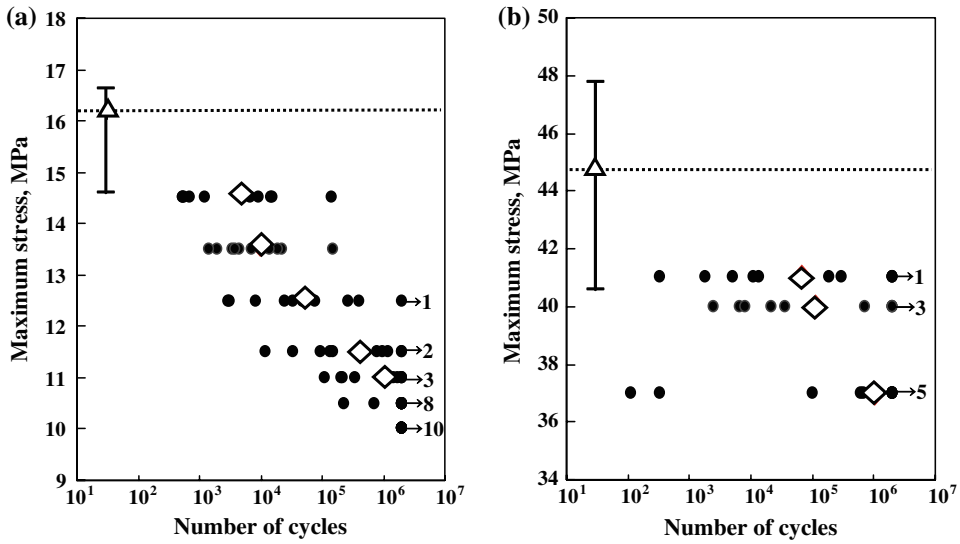

Fig. 5 Maximum stress as a function of the number of cycles to fracture during the cyclic fatigue tests of sample II at **a** room temperature and **b** 973 K. Open rhombic symbols indicate the median values of the apparent lifetime distributions. Filled circles indicate the fatigue data for the specimens that fractured during the tests, and the number of specimens that survived to the end of the tests are indicated by arrows pointing to the right with the corresponding number of specimens. Dotted lines indicate the median values of the flexural strength distributions

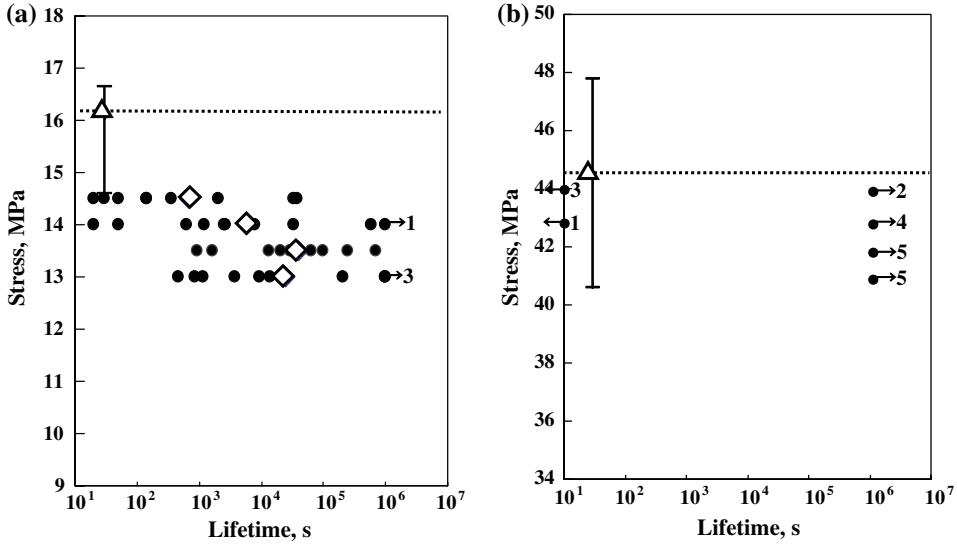

Fig. 6 Stress as a function of the lifetime to fracture during the static fatigue tests of sample II at **a** room temperature and **b** 973 K. Open rhombic symbols indicate the median values of the apparent lifetime distributions. Filled circles indicate the fatigue data for the specimens. Those with arrows pointing to the left indicate specimens that failed before their maximum stress was reached. The dotted lines, filled circles, and arrows pointing to the right with numbers have the same denotation as those in Fig. 5

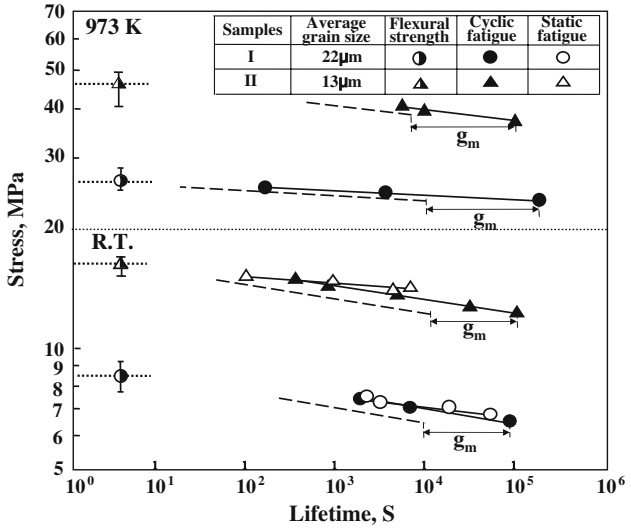

Fig. 7 Stress–lifetime curves obtained from the cyclic and static fatigue tests of samples I and II. The apparent lifetimes, corresponding to the number of cycles N, during the cyclic fatigue tests were determined by multiplying N and the cyclic period together

fatigue parameter. The dashed lines in Fig. 7 correspond to the modified cyclic fatigue data, which were calculated applying the g_m correction. By comparing the static and modified cyclic fatigue data, it is apparent that the fatigue lifetimes at room temperature are accelerated by application of the cyclic stress. Although all the specimens do not show static fatigue behavior at 973 K, the slopes of the modified cyclic fatigue stress lines are negative. This indicates that cyclic stress certainly accelerates the fatigue degradation at both temperatures.

Table 1 shows the static and cyclic fatigue parameters with the corresponding correlation parameters for the samples I and II. These parameters were determined from the slopes of the static and modified cyclic fatigue data shown in Fig. 7. The correlation coefficients are nearly equal to −1 for all the cases. The cyclic fatigue parameter for sample II at room temperature tends to be similar to that for sample I. Therefore, the effect of grain size on the cyclic fatigue parameters is comparatively smaller at room temperature. On the other hand, the cyclic fatigue parameter for sample II at 973 K is smaller than that for sample I. Therefore, this parameter at 973 K exhibits strong dependence on the microstructure.

Figure 8 shows typical SEM images of sample II fracture surfaces obtained from the cyclic fatigue test at room temperature ($\sigma_{max} = 11$ MPa, $N = 1.75 \times 10^6$). There are many debris from 2 to 5 μm in size in the semi-elliptical region (A) along the tensile side of the fractured surface, and no such debris in the surface (B) region, which is similar to the case of sample I reported previously [7, 8]. The debris were not observed on the fracture surfaces obtained by the flexural strength and static fatigue tests, but were formed only by the application of cyclic stresses. The AT ceramics have many microcracks along the grain boundaries at room temperature, resulting in grain bridging on the closed crack surfaces. The debris are probably produced by wear of the grains in the interlocking region behind the top of the main crack during application of cyclic stress. Region A is thought to correspond to a scar formed by subcritical growth of the main crack, accompanied by the formation of debris. If region A as shown in Fig. 8 is assumed to be a semi-elliptical pre-crack, the K_{IC} value corresponding to the pre-crack geometry [13] was calculated as 0.61 MPa $m^{-1/2}$. This is in good agreement with the value of 0.68 MPa $m^{-1/2}$ measured using the single-edge V-notched-beam (SEVNB) technique [11, 12], which could exclude stress shielding ability due to grain bridging. Therefore, this ability is thought to be dissipated by the wear of the interlocked grains during the cyclic

Table 1 Summary of fatigue parameters for samples I and II

Samples	Fatigue mode	Test temperature	Fatigue parameter	Correlation parameter
I	Cyclic	RT	19	−0.94
		973 K	82	−1.00
I	Static	RT	28	−0.97
		973 K	–	–
II	Cyclic	RT	21	−0.99
		973 K	52	−1.00
II	Static	RT	43	−0.89
		973 K	–	–

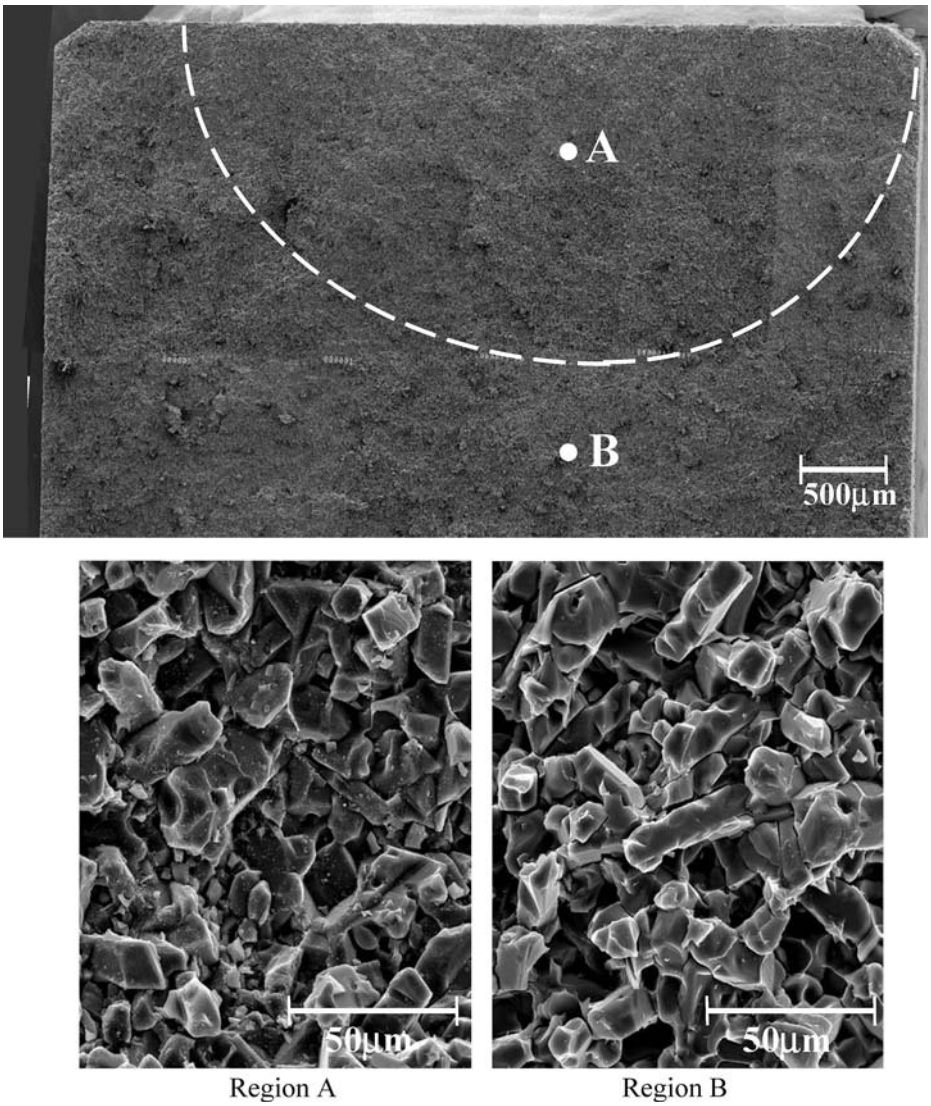

Fig. 8 SEM images of fracture surfaces of sample II that fractured during the cyclic fatigue test at room temperature ($\sigma_{max} = 11$ MPa, $N = 1.75 \times 10^6$)

fatigue tests. In other words, this suggests that the cyclic fatigue behavior is controlled by the grain bridging degradation mechanism [14].

Figure 9 shows typical SEM images of sample II fracture surfaces that failed during the cyclic fatigue test at 973 K ($\sigma_{max} = 37$ MPa, $N = 6.25 \times 10^5$). There are debris in the semi-elliptical region (A) along the tensile side of the fractured surface, and no debris in the surface (B) region, similar to that observed on the fracture surface shown in Fig. 8. The K_{IC}, calculated assuming the semi-elliptical region corresponds with a pre-crack formed by subcritical crack growth, was 1.19 MPa $m^{-1/2}$. This value is in good agreement with that of 1.12 MPa $m^{-1/2}$ measured by the SEVNB technique. For sample II at both

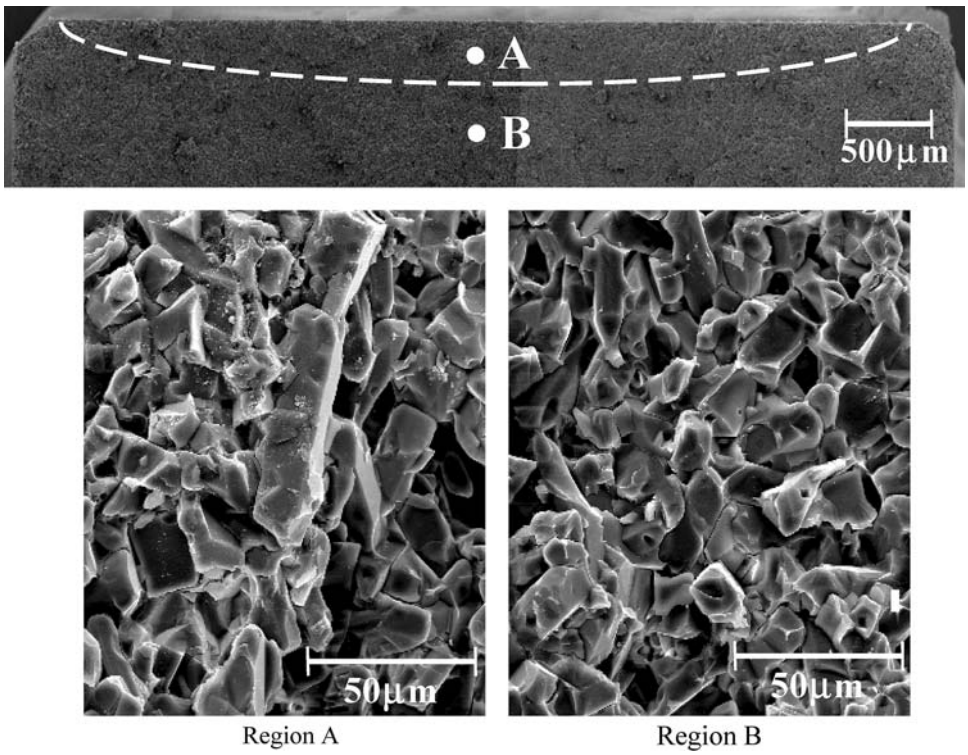

Fig. 9 SEM images of fracture surfaces of sample II that fractured during the cyclic fatigue test at 973 K ($\sigma_{max} = 37$ MPa, $N = 6.25 \times 10^5$)

room temperature and 973 K, the stress shielding capability is considered to disappear by the wear of the interlocked grains during the cyclic fatigue tests. The width of the region with the debris at 973 K was extremely narrower than that at room temperature, as shown in Figs. 8 and 9. The microcracks in the AT ceramics are strongly closed by thermal expansion of the grains at 973 K, compared to those at room temperature, so that a stress intensity factor at the tip of the main crack developed by the subcritical growth at 973 K should be larger than that at room temperature. Therefore, the morphology of the fracture surface at 973 K is probably related to the attainment of the factor to the critical value (K_{IC}) at slight crack growth. For sample I, as previously described, [7, 8] the unique scars on the fracture surfaces were developed by iterant self-healing and initiation of microcracks through a glass layer segregated at the crack surfaces during the cyclic fatigue tests at 973 K, where a part of the glass layer diffuses so as to decrease the total surface energy of the crack surfaces.

By contrast, such scars were hardly formed on the fracture surfaces during the cyclic fatigue tests at 973 K for sample II, which was prepared by increasing the SiO_2 content by several percent, compared to that of sample I; therefore, the softening temperature of the glassy grain boundary layers for sample II may be higher than that for sample I. Consequently, the cracks developed in sample II during the cyclic fatigue tests may be hardly restored compared to those in sample I, which results in the cyclic fatigue parameter for sample II at 973 K being smaller than that of sample I, as listed in Table 1.

Figure 10 shows the residual strength of the specimens that survived during the cyclic fatigue tests at room temperature as a function of the maximum applied stresses. The dotted lines indicate the median values of the flexural strength distributions tested in Ar at room temperature. These values are referred to as inert strength. The residual strength increases as the maximum stress decreases. The intersection of the lines of residual and inert strengths provides the statistical fatigue limit of the AT ceramics

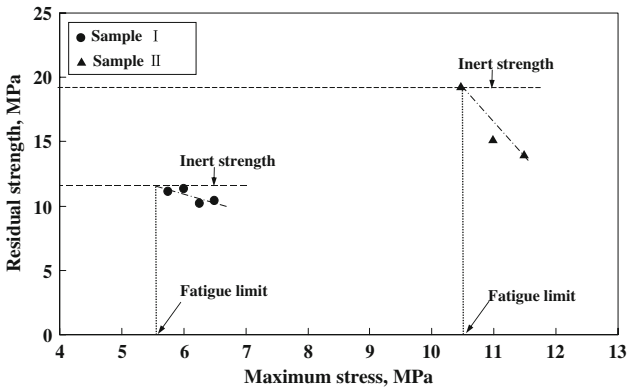

Fig. 10 Residual strength of the specimens that survived during the cyclic fatigue tests at room temperature as a function of maximum applied stresses. The dotted lines indicate inert strength of samples I and II

under the cyclic stresses applied at room temperature. The statistical fatigue limits of samples I and II were determined to be 5.5 and 10.5 MPa, respectively. The fatigue limit of sample II at room temperature is twice as large as that of sample I. The fatigue limit of the AT ceramics is increased corresponding to the increase in the flexural strength.

Effect of internal pores

Figure 11 shows the maximum stress as a function of the number of cycles to fracture during the cyclic fatigue tests of samples II and III at room temperature and 973 K. Open circles indicate the fatigue data for the sample III that fractured during the tests, and the number of specimens that survived to the end of the tests are indicated by arrows with the corresponding number of specimens. Rhombic symbols indicate the median values of the cycle fatigue distributions for samples II and III. The dotted lines indicate the median values of flexural strength distributions tested in air at room temperature. The median values of the cyclic fatigue distributions for samples II and III at room temperature are almost the same under any applied stresses. Therefore, there is little effect of internal pores on the fatigue properties of the AT ceramics at room temperature. On the other hand, at 973 K the median values of the cyclic fatigue distributions for sample III are almost half those for sample II under any applied stresses. The cyclic fatigue lifetime of the AT ceramics is obviously decreased at 973 K because of the presence of internal pores.

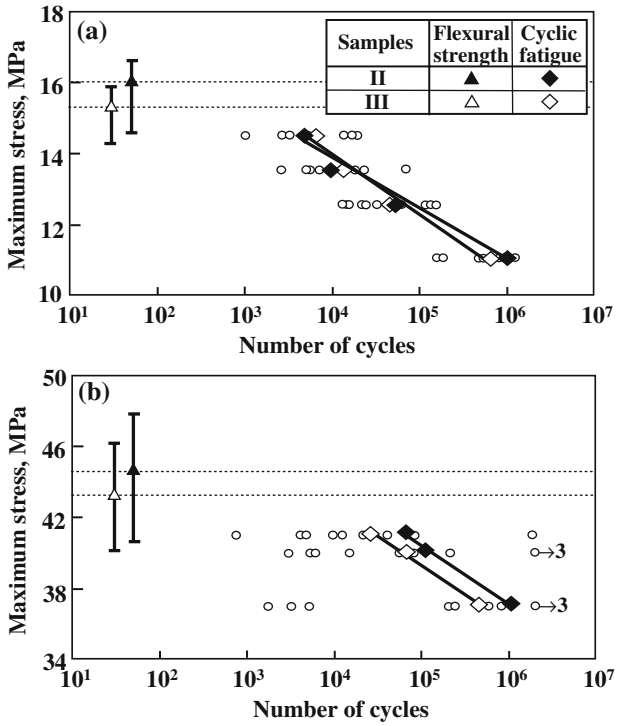

Fig. 11 Maximum stress as a function of the number of cycles to fracture during the cyclic fatigue tests of samples II and III at **a** room temperature and **b** 973 K. Open circles indicate the fatigue data for sample III that fractured during the tests, and the number of specimens that survived to the end of the tests are indicated by arrows pointing to the right with the corresponding number of specimens. Rhombic symbols indicate the median values of the cycle fatigue distributions for samples II and III. Dotted lines indicate the median values of flexural strength distributions

Figure 12 shows SEM images of sample III fracture surfaces from the cyclic fatigue test at room temperature ($\sigma_{max} = 11$ MPa, $N = 1.87 \times 10^5$). Arrow indicates one of a large number of the internal spherical pores introduced during the slip-casting of sample III. Many debris are observed in the semi-elliptical region (A) along the tensile side of the fractured surface, similar to the fracture morphology for sample II shown in Fig. 8. The AT ceramics already have many intergranular microcracks that are connected to each other, which results in the formation of large cracks at room temperature; therefore, the effect of pores on the fracture behavior at room temperature is thought to be negligibly small.

Figure 13 shows SEM images of sample III fracture surfaces from the cyclic fatigue test at 973 K ($\sigma_{max} = 41$ MPa, $N = 7.49 \times 10^2$). There are regions where debris exist on the fracture surface and areas where debris are absent, similar to that observed at room temperature, as shown in Fig. 12. However, the shape of the observed region containing debris (the broken line) in Fig. 13 is remarkably different from that of sample II without the pores introduced by slip-casting, as shown in Fig. 9, and the region is partially formed far deeper from the tensile surface. In particular, there is significantly a large amount of debris in the regions enclosed by dotted lines, as shown in the region A of Fig. 13. These regions always have the pores introduced by slip-casting. The raw powders and sintering additives used for sample III were the same as those used for sample II, so that the chemical composition of the grain boundary layers and/or the grain size are identical to each other, and only the amount of pores present in the samples is varied. Therefore, the microcracks are probably strongly closed at 973 K for sample III, but may not adhere to each other through the glassy grain boundary layer in a similar way to that in sample II. The forced deformation of the specimens due to the applied cyclic stresses is caused by an accumulation of the slight shift in each interlocked grain. This shift is thought to progress mainly around the pores, where the apparent elastic modulus is locally small, resulting in acceleration of the wear of the grains enclosing pores and subsequent large crack formation. The amount of defects, such as pores, should therefore be eliminated as much as possible from

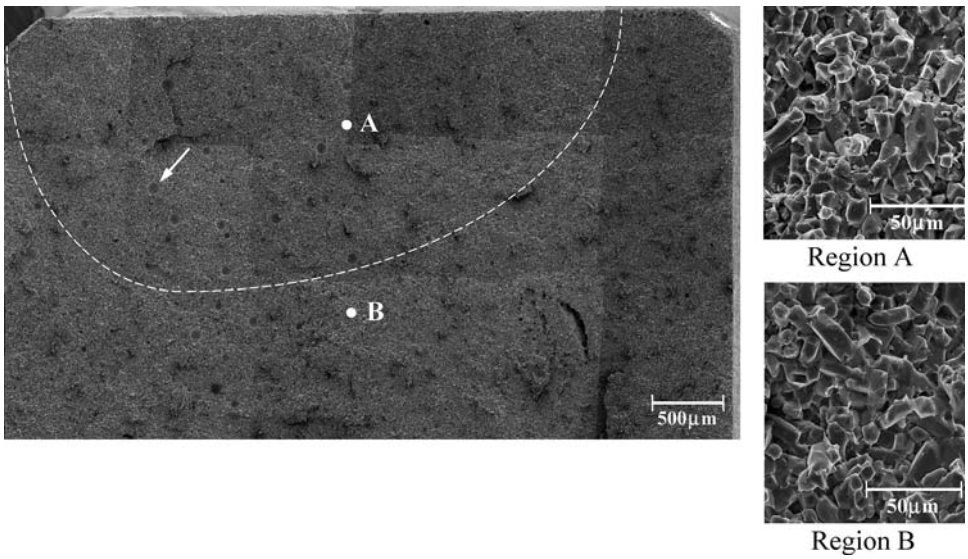

Fig. 12 SEM images of sample III fracture surfaces from the cyclic fatigue test at room temperature ($\sigma_{max} = 11$ MPa, $N = 1.87 \times 10^5$). Arrow indicates one of a large number of the internal spherical pores introduced during the slip-casting of sample III

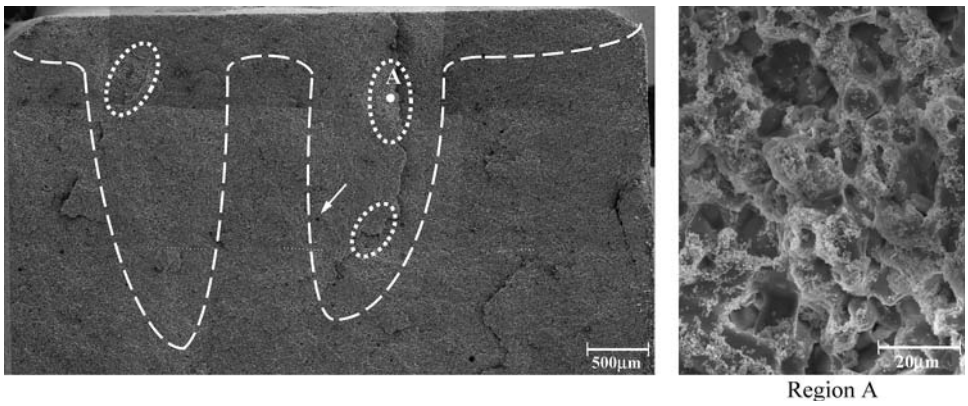

Fig. 13 SEM images of sample III fracture surfaces from the cyclic fatigue test at 973 K ($\sigma_{max} = 41$ MPa, $N = 7.49 \times 10^2$). Arrow indicates one of a large number of the internal spherical pores introduced during the slip-casting of sample III

AT ceramics to be utilized as casting parts in contact with molten aluminum alloys.

Conclusions

A decrease in the grain size of AT ceramics leads to a decrease in the size and amount of microcracks present at the grain boundaries, resulting in an increase of the flexural strength at room temperature and 973 K. Fatigue degradation was accelerated by the application of cyclic stresses at both temperatures. The statistical cyclic fatigue limit at room temperature was raised by decreasing the grain size, which corresponds to an increase in the flexural strength. The cyclic fatigue behavior of the sample with smaller grains was considered to be controlled mainly by the grain bridging degradation mechanism at all the temperatures. However, the cyclic fatigue behavior of the sample with larger grains was changed depending on the testing temperatures. Although there was little effect of internal pores on the cyclic fatigue behavior of the AT ceramics at room temperature, the cyclic fatigue life time at 973 K was obviously decreased by the existence of internal pores.

References

1. Kitaoka S (2003) Ceramics 38:283
2. Thomas HAJ, Stevens R (1987) Brit Ceram Trans J 88:144
3. Morosin B, Lynch RW (1972) Acta Cryst B28:1040
4. Ohya Y, Nakagawa Z, Hamano K (1987) J Am Ceram Soc 70:C184
5. Ohya Y, Nakagawa Z (1996) J Mater Sci 31:1555. doi:10.1007/BF00357864
6. Jin G, Honjoh A, Awaji H (2000) J Ceram Soc Jpn 108:614
7. Matsudaira T, Kitaoka S, Kuzushima Y, Awaji H, Igimi D (2004) J Soc Mat Sci 53:607
8. Matsudaira T, Kuzushima Y, Kitaoka S, Awaji H, Yokoe D (2004) J Ceram Soc Jpn 112:S327 (Suppl, 112–1, PacRim5 Special Issue)
9. Japan Industrial Standard (1997) Test methods of thermal diffusivity, specific heat capacity, and thermal conductivity for fine ceramics by laser flash method. JIS R 1611, UDC 666.59:536.2, Japan Standards Association, Tokyo, Japan

10. Japan Industrial Standard (1989) Testing methods for elastic modulus of high performance ceramics at elevated temperatures. JIS R 1605, UDC 666.59:620.173.22, Japan Standards Association, Tokyo, Japan
11. Awaji H (2001) Strength of ceramic materials (Serammiku-Zairyokyodogaku). Corona Publishers Co. Ltd, Tokyo, Japan, p 71
12. Awaji H, Choi S-M, Jayaseelan DD (2001) J Ceram Soc Jpn 109:591
13. Newman JC Jr, Raju IS (1981) Eng Fract Mech 15:185
14. Grathwohl G (1988) Mat wiss Werkstofftech 19:113